RFP-3683
April 3, 1985

RFP-3683
April 3, 1985

THE TERRAIN–RESPONSIVE ATMOSPHERIC CODE (TRAC) FOR PLUME GROWTH AND DISPERSION IN COMPLEX TERRAIN

C. Reed Hodgin

Rockwell International

North American Space Operations
Rocky Flats Plant
P.O. Box 464
Golden, Colorado 80402-0464

U. S. DEPARTMENT OF ENERGY
CONTRACT DE-AC04-76DPO3533

Printed in the United States of America
Available from the
National Technical Information Service
U.S. Department of Commerce
Springfield, Virginia 22161
Price Code: 001-050 pages, Code A02
Price Code: 026-050 pages, Code A03
Price Code: 051-075 pages, Code A04
Price Code: 076-100 pages, Code A05
Price Code: 101-125 pages, Code A06

DISCLAIMER

Printed
April 3, 1985

M85010541

RFP--3683

DE85 010541

RFP-3683
UC-11 ENVIRONMENTAL CONTROL
TECHNOLOGY AND
EARTH SCIENCES
DOE/TIC-4500 (Rev. 73)

THE TERRAIN–RESPONSIVE ATMOSPHERIC CODE (TRAC) FOR PLUME GROWTH AND DISPERSION IN COMPLEX TERRAIN

C. Reed Hodgin

R. L. Thomas, Editor

I. C. Delaney, Compositor

DISCLAIMER

ROCKWELL INTERNATIONAL
NORTH AMERICAN SPACE OPERATIONS
ROCKY FLATS PLANT
P.O. BOX 464
GOLDEN, COLORADO 80402-0464

Prepared under Contract DE-AC04-76DP03533
for the
Albuquerque Operations Office
U.S. Department of Energy

CONTENTS

THE TERRAIN–RESPONSIVE ATMOSPHERIC CODE (TRAC) FOR PLUME GROWTH AND DISPERSION IN COMPLEX TERRAIN

C. Reed Hodgin

ABSTRACT

Use of atmospheric dispersion models to assess pollutant impacts in complex terrain is increasing. However, the temporally and spatially varying wind and turbulence fields in mountainous areas often invalidate the assumptions of straight-line flow and horizontal homogeneity inherent in standard plume models. A dispersion model was recently developed at the Rocky Flats Plant to realistically simulate dispersion processes in complex terrain.

The new model treats pollutant releases as a series of overlapping ellipsoidal puffs. The ends of each puff axis are defined by "tracer" particles, which are independently advected through the modeled windfield. The puff axes are not, in general, orthogonal. Thus, a puff can develop an arbitrary shape in response to differential diffusion rates, horizontal convergence and divergence, vertical shear, surface reflection, and gravitational settling.

The model includes modules for puff transport, diffusion, wet and dry deposition, resuspension, surface roughness effects, ingrowth, decay, and external and internal dosimetry. This report focuses on the simulation of puff growth and shape.

INTRODUCTION

Atmospheric dispersion models are increasingly being utilized in air quality assessments. Models are most useful in applications where direct atmospheric monitoring is not possible—e.g., facility planning, regulatory assessment of proposed sources, and interpolation among sparse observational data. Dispersion modeling is also an important tool in emergency response. Rapid predictions of the impacts of unplanned releases can make crucial mitigative measures possible.

The modeling approach most widely used during the last 25 years is the straight-line Gaussian model. This approach assumes horizontal homogeneity and steady-state atmospheric conditions. The result is a straight, infinite plume path with a Gaussian distribution of mass in all directions from the centerline. Many models currently employ the straight-line Gaussian concept.[1–4]

Growing numbers of modeling studies are being conducted in complex terrain, where mountain-valley and channeled flows are prevalent. The space- and time-varying windfields associated with these flows invalidate the straight-line Gaussian approach. Plume paths in complex terrain are often substantially nonlinear[5] and can exhibit non-Gaussian mass distributions.[6] These problems can result in overwhelming errors in ground level concentration estimates. In particular, the straight-line concept can lead to centerline misplacements of many horizontal standard deviations, resulting in order-of-magnitude errors in concentrations near the plume path.

Much effort has been focused recently toward improving complex terrain models. Field, laboratory, and mathematical studies significantly advanced our understanding of the processes that affect transport and dispersion in mountainous areas. Results of these studies are now becoming available for use in applied dispersion models.

ELLIPSOIDAL PUFF APPROACH

One method for simulating pollutant transport and growth in a varying flow field is the Gaussian puff model. In this approach, puffs of material are

released and allowed to travel independently through the flow. A puff-following (Lagrangian) coordinate system allows each puff to move along a nonlinear trajectory and grow at varying rates. A single puff simulates an instantaneous release, while a continuous plume is modeled by the sequential release of overlapping puffs.

The standard puff model is limited by the requirement of symmetry about the puff axes. Puffs are usually assumed spherical with identical growth rates in all directions.

Sheih[7] developed an ellipsoidal puff model to overcome these restrictions for the special conditions associated with lake-shore flow systems. The Sheih model allows different growth rates along the puff axes and accounts for the stretching effects of vertical wind shear. The model operates by placing six tracer "particles" around the envelope of each puff. The particles are tracked through the windfield and an ellipsoid fitted to them at each time step. The axes of the ellipsoid remain orthogonal. The x and y axes rotate with time, while the z axis remains vertical. Symmetry is required about each plume axis.

TRAC MODEL

A more generalized ellipsoidal puff model called the Terrain–Responsive Atmospheric Code (TRAC), has been developed at the Rocky Flats Plant. Each puff is defined (as described in the preceding section) by six tracer particles. However, in the TRAC model, the particles define the edges of the puff ($\pm 3\sigma$) along each of the axes. The particles are advected through a three-dimensional windfield, which includes the complex terrain effects of advection, vertical shear, horizontal divergence and convergence, and lofting. The locations of the particles at each time step define a new set of axes for the puff. These axes are not constrained to be orthogonal; thus, the puff assumes an arbitrary shape in response to varying flow and dispersion conditions throughout its volume. For instance, a vertically increasing wind speed profile will result in nodes in the puff shape at the top downwind edge and at the bottom upwind edge. These nodes will rotate around the puff as it moves through the varying flow field.

The TRAC model also includes the effects of plume rise, surface reflection, particulate settling, dry deposition of gases and particulates, rain-out and wash-out, varying surface roughness, and spatially and temporally varying stability conditions. The code will be used to simulate releases of radionuclides as well as non-nuclear materials, and thus will treat phenomena such as ingrowth and decay, plumeshine, and internal dose commitment.

This report focuses on the model's scheme for determining puff growth and shape.

COORDINATE SYSTEMS

The TRAC model works simultaneously in three different coordinate systems (Figure 1). The x, y, z system is a standard Eulerian reference frame,

FIGURE 1. Coordinate Systems Used by the TRAC Model

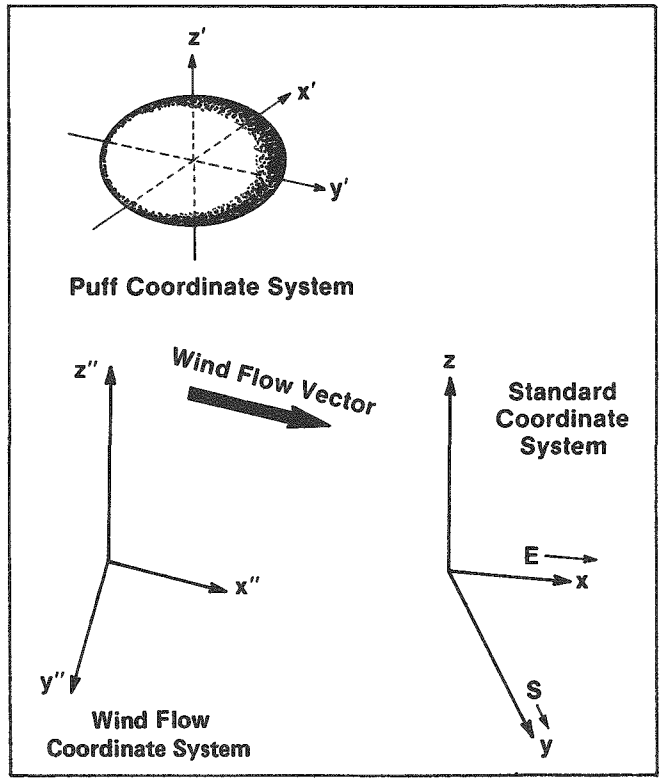

where x is a horizontal west-east axis, y is a horizontal south-north axis, and z is a vertical axis. Universal transverse mercator coordinates are utilized for the horizontal axes, while meters above mean seal level are used for vertical coordinates. This system is referenced when calculating wind flow fields, tracking the tracer particles, and determining puff effects on selected receptors.

The model also uses a "wind flow" coordinate system with a puff-following, Lagrangian reference frame. In this system, the x'' axis is horizontal and parallel to the local wind flow vector, the y'' axis is horizontal and perpendicular to the local wind flow vector, and the z'' axis is vertical. This coordinate system is used by the model in calculating local dispersion rates for a puff.

The third reference frame employed by the model is an internal puff coordinate system. This system is also Lagrangian, following a puff through the study region. The puff coordinate system is not orthogonal; the three axes are arbitrary and may tilt at any angle to each other. The axes are defined by the tracer particle locations at each time step and rotate and translate throughout the puff's existence. The local puff coordinate system defines the puff's shape and size (combining the effects of divergence/shear with dispersion). It also determines a receptor's position relative to the puff centroid.

PUFF RELEASES

A spherical puff model must generate many puffs to simulate a plume release. Otherwise, fictitious gaps occur in the plume near the source. Using the ellipsoid approach, the TRAC model generates elongated plume segments, which realistically simulate a continuous release with many fewer puffs. The rate at which puffs are generated is dependent on the basic time step input for the model run. This time step is the period over which meteorological and source characteristics are assumed quasi-steady-state. The time step is user-selectable with a default value of 15 minutes.

Unrealistic behavior in the plume centerline concentration is avoided by generating three overlapping puffs during each time step. As shown in Figure 2, the resulting centerline trend approaches the usual Gaussian distribution much more closely than if a single puff is generated during each step.

The initial size and shape of a puff is determined by the conditions near the source at the time of release. The x' axis is set parallel to the wind flow vector at the location and height of the source with an initial length of $\Delta X'$, where $\Delta X'$ is the greater of the spread caused by advection,

$$\Delta X' = U_p \frac{\Delta t}{2} \quad , \qquad (1)$$

FIGURE 2. Initial Centerline Concentration Profile of a Plume Segment Represented by Three Overlaid Puffs

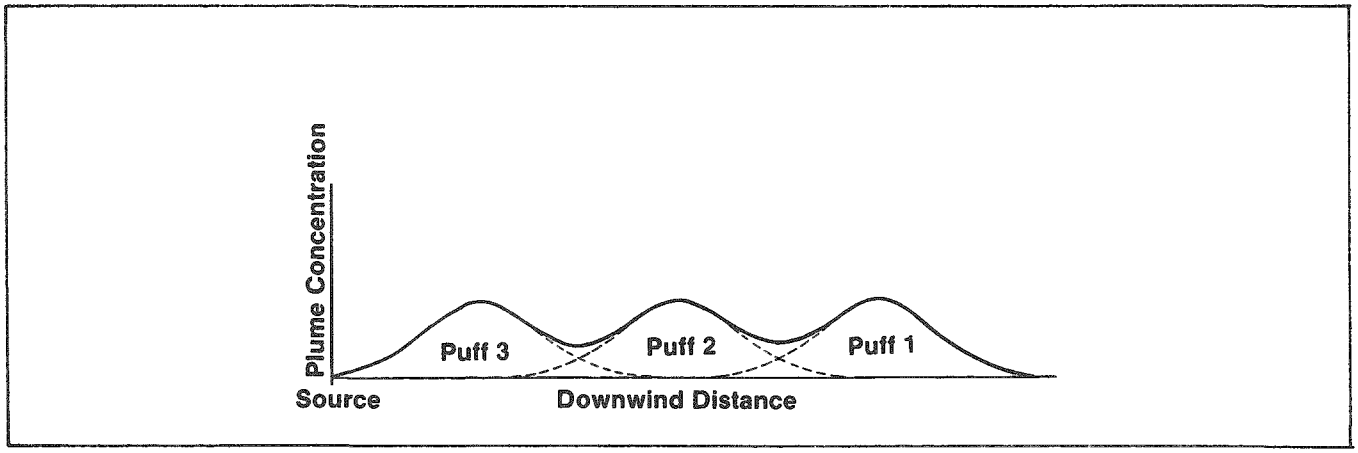

or diffusion,

$$\Delta X' = 3\Delta t \frac{d\sigma_x}{dt} \qquad (2)$$

Here, U_p is the wind speed at the emission height, $\frac{d\sigma_x}{dt}$ is the along-wind diffusion rate near the source, and Δt is the basic time step. This allows the puff to grow longitudinally through diffusion alone if conditions are calm. The particle positions are adjusted vertically for plume rise and gravitational settling after all three puffs have been generated. The resulting x′ axis may then tilt from the horizontal. A release period of one half the basic time step is assumed for longitudinal spread to produce the desired puff overlap.

The y′ axis is defined by the crosswind dispersion that takes place during the puff release period ($\Delta t/3$),

$$\Delta Y' = 2\Delta t \frac{d\sigma_y}{dt} \quad , \qquad (3)$$

where $\Delta Y'$ is the length of the y′ axis and $\frac{d\sigma_y}{dt}$ is the crosswind diffusion rate near the source. No divergence effects are treated at this time. The initial y′ axis is horizontal since the effects of plume rise and gravitational settling affect both ends of the y′ axis equally.

The z′ axis is defined by the vertical dispersion that takes place during the release period,

$$\Delta Z' = 2\Delta t \frac{d\sigma_z}{dt} \quad , \qquad (4)$$

where $\Delta Z'$ is the length of the z′ axis and $\frac{d\sigma_z}{dt}$ is the vertical diffusion rate. No divergence effects are treated at this time, but gravitational settling and plume rise are included.

The z′ particles are allowed to travel below local ground level. Conservation of mass is ensured through reflection terms included in the dispersion calculation. Tracer particles, which have been placed below the surface, are advected at a speed appropriate to one meter above ground level.

The three puffs generated during a time step are positioned evenly along the wind flow vector with the leading edge of the first puff at a distance $1.25\ U_p\ \Delta t$ from the source (to provide overlap between time steps) and the rear edge of the third puff at the source location. The vertical position of each tracer particle is adjusted for the plume rise and settling that occur during travel to its designated location. Thus, the puffs may occupy different vertical positions and may exhibit different tilts in their x′ axes. Figure 3 is a representation of a plume at the end of the first time step.

FIGURE 3. Model Representation of a Plume at End of First Time Step

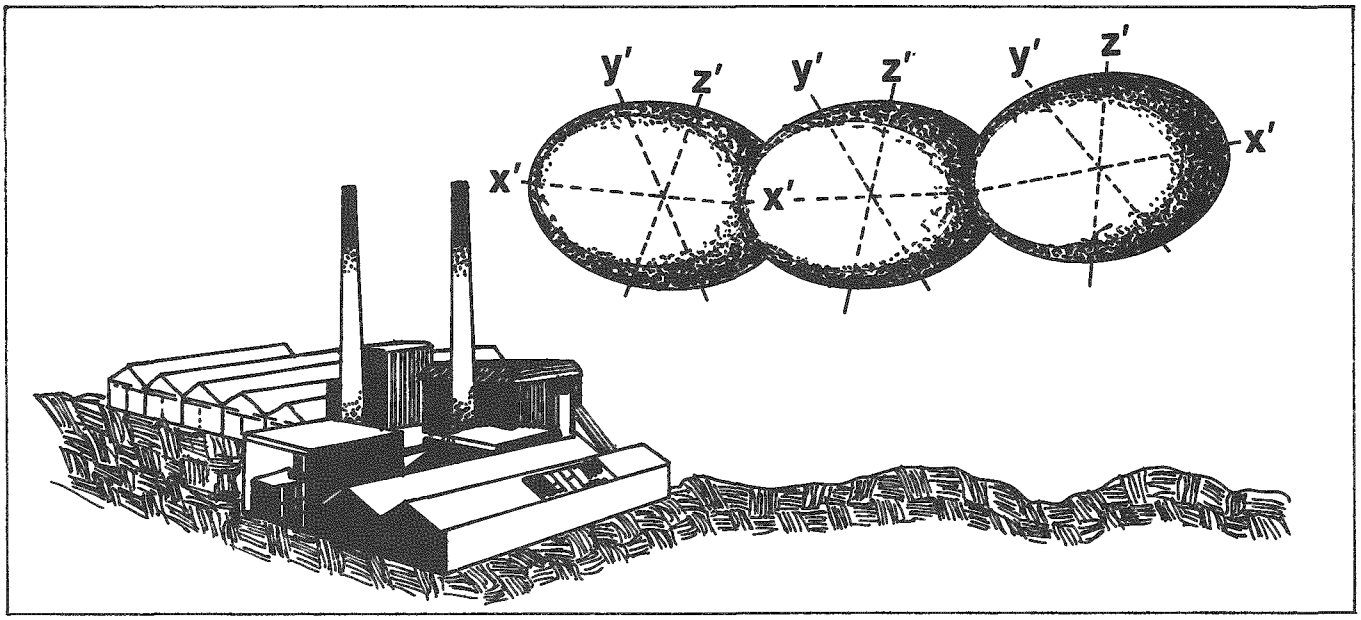

WIND FIELD PARAMETERIZATION

Critical to a puff's transport and growth is a realistic representation of the nearby flow field. The model builds windfields based on surface and upper air observations, then includes the effects of terrain channeling, thermal forcing, and varying surface roughness. This allows the code to realistically reproduce complex terrain phenomena such as diurnal mountain-valley flows, lee-slope winds, orographic uplifting, synoptic forcing, vertical shear, and horizontal divergence and convergence.

Because air flow patterns exhibit large vertical variations over complex terrain, a four-layer windfield model is employed (Figure 4). Wind vector profiles are calculated from the surface to the gradient layer for all grids affected by a puff. Pollutant trajectories are developed by overlaying successive windfields.

Mixing Depth

The mixing depth, or the top of the mixing layer, is defined as the discontinuity, which inhibits upward transport of puff material from the surface layer. This level corresponds to the top of the surface-based radiational inversion during stable conditions,[8] and to the bottom of the first inversion aloft during neutral and unstable conditions.[9]

A first estimate of the mixing depth is determined for each grid by comparing the surface elevation against the height of the inversion level. The mixing depth is not a horizontal surface over complex terrain, but responds slowly to varying topography. The model treats this effect by performing an additional analysis to estimate the microscale mixing depth structure over individual grids.

FIGURE 4. Four-Layer Approach Used by the TRAC Model for Vertical Wind, Temperature, and Diffusion Profiles. Shown are typical layer depths and potential temperature and wind speed profiles for stable (nighttime) conditions.

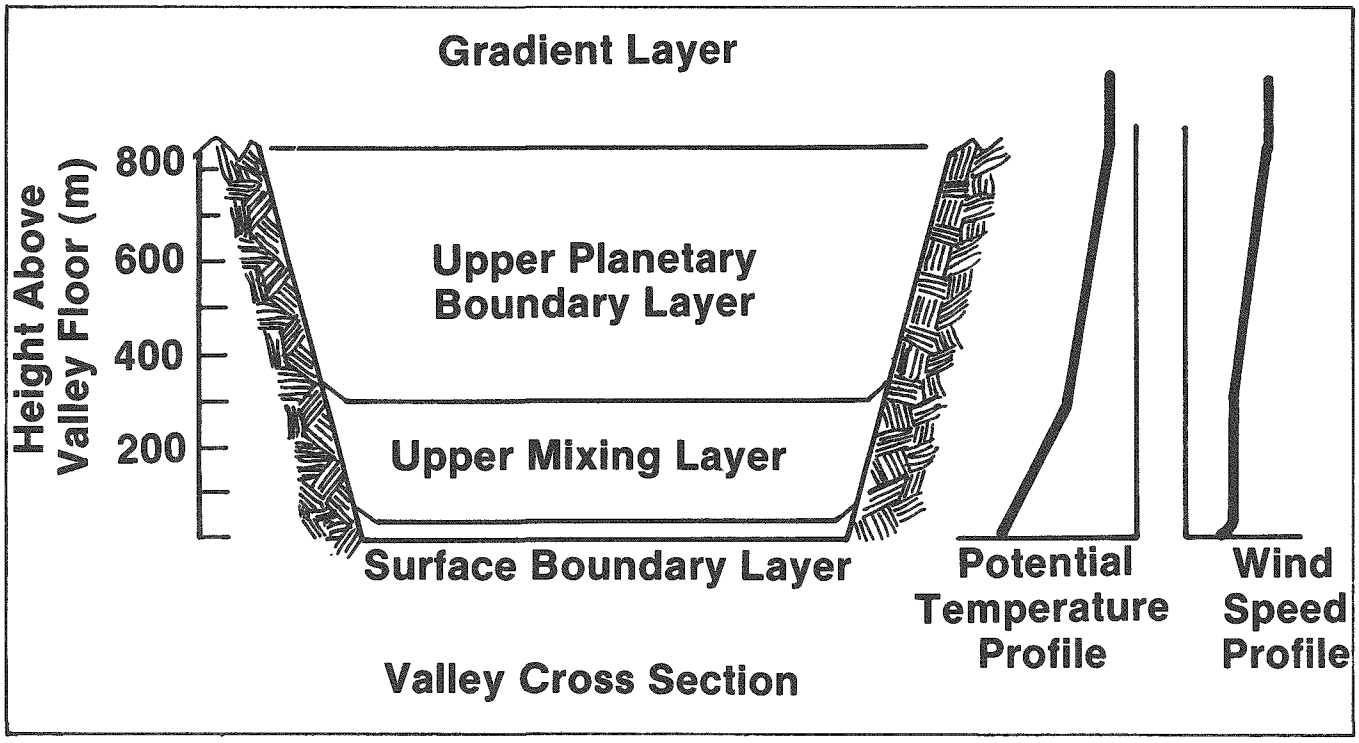

If the potential temperature at the grid surface is greater than that at the inversion height, then the grid is above the inversion layer. A large default mixing depth is assigned to the grid. If the grid potential temperature is lower than the temperature at the inversion layer height, then the grid is below the inversion marking the top of the mixed layer. In this case, the greater of the observed inversion height or a default value of 10 meters is assigned to the mixing depth. Thus, the model can respond to local areas of stable air embedded in larger scale neutral or unstable regions.

Surface Boundary Layer

The Surface Boundary Layer is the layer of constant shear stress immediately above the surface. The top of the Surface Boundary Layer is defined by the Monin-Obukhov length during stable conditions and as 10% of the mixing depth under neutral and unstable conditions.[10]

A modified version of the National Forest Service's WINDS model characterizes the windfield in this layer.[11] Combining two single-layer models that separately consider terrain influences[12] and thermally driven flows,[13] the WINDS code is a mass-conservative model based on simplified forms of the divergence and vorticity equations. The model also considers frictional effects.

Available wind and temperature observations are interpolated to each grid, then modified to produce a nondivergent flow field. Thermal, topographic, and frictional disturbances are superimposed on the underlying flow, resulting in a stream function and a velocity potential for each grid. The code outputs potential temperature and vector components of surface friction velocity for each model grid.

The WINDS model outputs are used to develop an individual Surface Boundary Layer wind profile over each grid. Wind direction is assumed constant with height in this layer. Wind speed shears vertically with a log-linear profile:[14]

$$U = \left(\frac{u_*}{k}\right)\left\{\ln\left(\frac{z}{z_0}\right) + \ln\left[\frac{(\zeta_0^2 + 1)\ (\zeta_0 + 1)^2}{(\zeta^2 + 1)\ (\zeta + 1)^2}\right] + 2\left[\tan^{-1}(\zeta) - \tan^{-1}(\zeta_0)\right]\right\}, \quad (5)$$

where U is the wind speed, u_* is the surface friction velocity, k is Von Karman's constant, z is the height above the ground surface, and z_0 is the surface roughness height. The two similarity parameters are calculated as

$$\zeta = \left(1 - \frac{\gamma z}{L}\right)^{1.25} \quad (6)$$

and

$$\zeta_0 = \left(1 - \frac{\gamma z_0}{L}\right)^{1.25} \quad (7)$$

where γ is an empirical constant and L is the Monin-Obukhov scaling length. The surface roughness length is related to surface characteristics on a grid-by-grid basis. Monin-Obukhov scaling length and surface friction velocity are discussed in a subsequent section, "Puff Growth by Diffusion."

The model generates terrain-following flow for the Surface Boundary Layer. However, winds in complex terrain express inertia; flow does not exactly respond to small topographic features or extreme elevation gradients. This effect is reproduced in the model by requiring trajectories to follow locally smoothed terrain. The "smoothed" elevation of each grid is determined by averaging the elevations of the current grid, the grid most recently encountered, and the next grid along the current vector. This results in a sliding smoothed path and allows a trajectory to approach or loft away from abrupt terrain variations.

Upper Mixing Layer

The Upper Mixing Layer is defined in the model as that portion of the mixing layer above the Surface Boundary Layer. The bottom of the Upper Mixing Layer coincides with the top of the Surface Boundary Layer. This layer extends to the top of the mixing depth—ranging from a few hundred meters above the surface in stable conditions to 1,000 or more meters during unstable periods. Its height is not allowed to exceed the gradient level.

Field studies show that wind speed in the Upper Mixing Layer is nearly constant, while direction shears steadily with height.[10] This effect is simulated in the model by calculating the speed at the

top of the Surface Boundary Layer and holding it constant through the Upper Mixing Layer. Direction shear is introduced by allowing the ratio (v/u) to smoothly approach that of the gradient level.

Because the Upper Mixing Layer is coupled to the surface, terrain-following trajectories are developed by the model for this layer. The increased separation between this layer and the ground surface results in greater inertia for flow over terrain obstacles than is experienced in the Surface Boundary Layer. This effect is modeled by calculating sliding elevation averages from nine adjacent grids to produce a highly smoothed path for trajectory calculation. Thus, a trajectory in the Upper Mixing Layer will ignore small-scale terrain features.

Recent field studies indicate that plumes emitted into the Upper Mixing Layer during down-slope or down-valley flow tend to lift away from the surface and gently descend the slope.[15] The model recreates this phenomenon by maintaining a trajectory at a constant percent penetration into the Upper Mixing Layer. As the Upper Mixing Layer deepens with movement into or along the valley, the trajectory moves proportionately higher above the surface (Figure 5).

Upper Planetary Boundary Layer

Over flat terrain, the top of the Upper Mixing Layer corresponds to the top of the Planetary Boundary Layer and defines the maximum vertical extent of surface effects on air flow. However, complex terrain affects flow patterns to the top of the valley wall, which often exceeds the mixing depth.[16] The TRAC model accounts for these effects with a third vertical layer, termed the Upper Planetary Boundary Layer.

FIGURE 5. Typical Plume Path in the Upper Mixing Layer During Down-Slope or Down-Valley Flow. Note that the plume gradually lofts away from the descending slope.

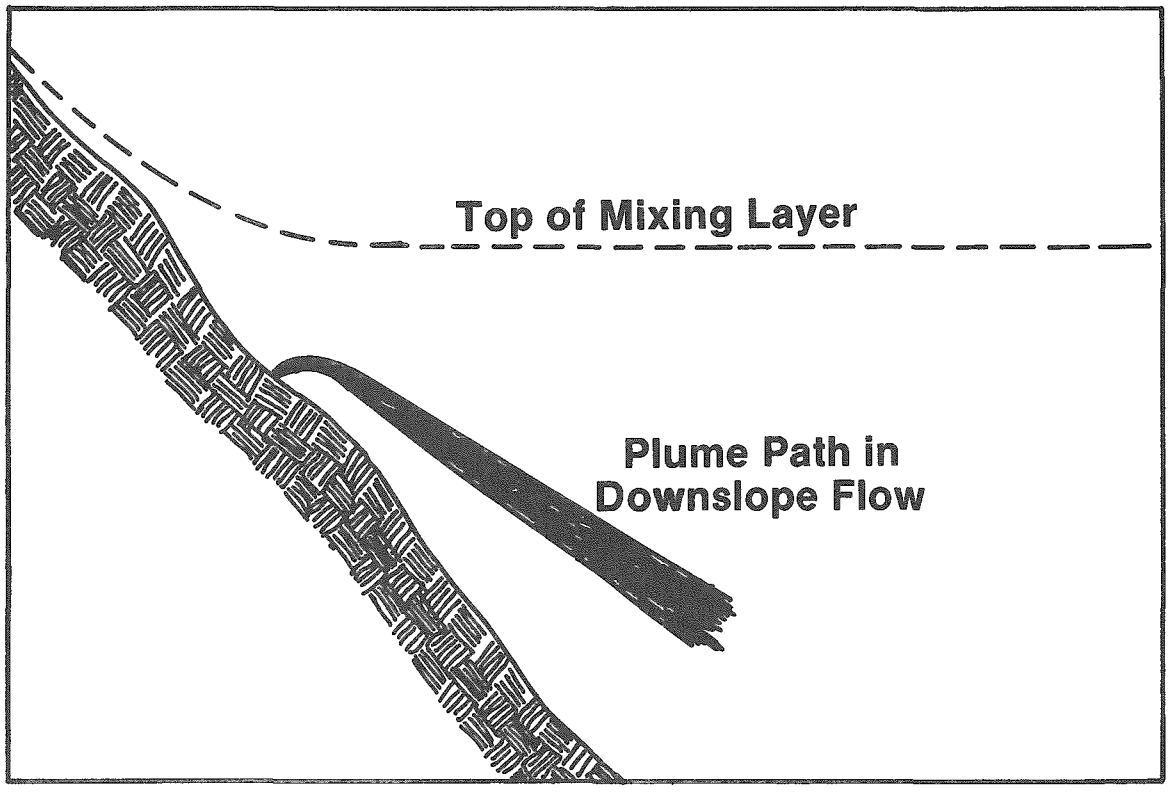

The bottom of the Upper Planetary Boundary Layer coincides with the inversion marking the top of the Upper Mixing Layer (mixing depth). The Upper Planetary Boundary Layer extends to the gradient level. The Upper Planetary Boundary Layer locally disappears if the mixing depth exceeds the height of the valley wall.

Horizontal wind components in the Upper Planetary Boundary Layer are allowed to change smoothly with height, approaching the gradient wind vector at the top of the layer. Both speed and direction shear occur in the Upper Planetary Boundary Layer.

Vertical motion in the Upper Planetary Boundary Layer is not coupled to terrain features below. Instead, trajectories maintain a constant vertical penetration into the layer, deviating from the horizontal only as the thickness of the layer varies.

Gradient Layer

The Gradient Layer includes all regions above the gradient level—the height at which surface and terrain effects no longer impact flow. The gradient level is defined by the model as the greater of the valley wall elevation or the mixing depth. The top of the gradient layer is unrestricted.

Because the model treats a mesoscale, rather than synoptic, study region, the gradient level wind direction and speed are assumed horizontally and vertically constant throughout the layer. Trajectories above the gradient level are constrained to isentropic surfaces,[17] which in this version of the model are horizontal.

PUFF GROWTH BY DIVERGENCE/SHEAR

The wind vector profile developed for each affected grid is held constant for a complete time step, then updated as new meteorological observations become available.

Each puff tracer particle is independently advected through the varying windfield, resulting in non-linear trajectories for different portions of a puff. The full resolution of the windfield is retained by allowing a particle to change direction and speed each time it moves into a new grid. (Most models assign a single weighted vector, held constant for an entire time step.)

Puff growth caused by horizontal divergence and vertical shear is determined through comparison among tracer particle trajectories (Figure 6). Positions are calculated at the midpoint of a time

FIGURE 6. Model Puff Showing the Six Tracer Particles Which Define the Non-Orthogonal Axes. Puff shape is dynamically defined by calculating independent trajectory for each particle.

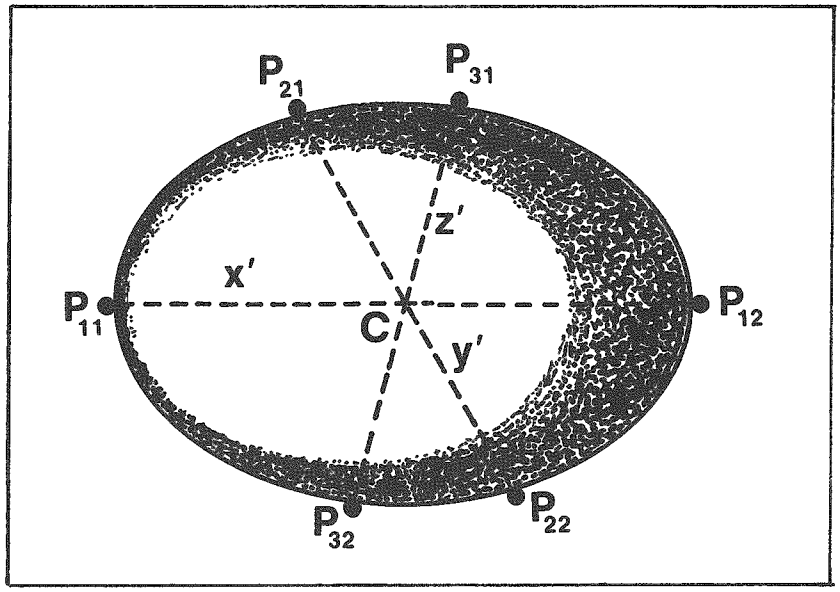

step for the six particles defining a puff. These positions determine the vectors of the local puff axes. Next, the axes are translated until they meet at a best-fit intersection, which defines the centroid of the puff. The lengths of the axes represent $\pm 3\sigma$, describing the pollutant distribution in each local puff dimension. The latest sigmas are compared to those calculated at the midpoint of the previous time step to define the divergence/shear expansion rate. Negative growth rates (convergence) are allowed at this step, but are removed when diffusion is considered.

PUFF GROWTH BY DIFFUSION

Puff diffusion is evaluated in the wind-flow (x″, y″, z″) coordinate system, defined by the horizontal wind vector at a puff's centroid. The along-flow diffusion coefficient is parallel to the local flow, while across-flow diffusion is evaluated in the direction perpendicular to the flow direction. Vertical diffusion is calculated in the vertical plane.

The theory of puff diffusion is not sufficiently developed to allow application of direct puff diffusion formulas in operational models. Therefore, diffusion coefficients developed for plume simulation are used in the TRAC model. This approach is reasonable for moderate and longer travel times or when using puffs to simulate continuous releases. Underestimates of diffusion rates can result for single puff releases at small travel times.

The plume diffusion formulas selected for the TRAC model are Eurlerian in nature and treat steady-state transport. They have been converted to a Lagrangian reference frame by differentiation with respect to time. In this form, the model calculates a local rate of change of diffusion for a puff based on its time since release.

New diffusion rates are determined for each puff during each time step. The total diffusion during a time step is calculated by multiplying the differential diffusion rate by the length of the time step.

Similarity Approach

Much of the recent effort in dispersion research centers on refining similarity approaches to diffusion.[18,19,20] The results are sufficiently complete so that similarity-based dispersion can replace the traditional Pasquill-Gifford-Turner approach.[21]

The TRAC model utilizes grid-by-grid values of Monin-Obukhov scaling length and surface friction velocity to characterize thermally and frictionally driven diffusion. Similarity concepts are employed directly for the Surface Boundary Layer, and are semi-empirically extended upward to the mixing depth. Observations and theoretical treatments of diffusion above the mixing layer are not complete enough for use in applied modeling. Because of this, the TRAC model applies the diffusion rate calculated for the top of the mixing layer to all higher levels.

Monin-Obukhov Stability Scaling Length

Monin-Obukhov length is determined for each grid using modeled potential temperature and wind conditions to characterize thermal and frictional turbulence. The Bulk Richardson Number is calculated as discussed by Draxler:[22]

$$B = \frac{gz^2}{\overline{T}} \quad \frac{\Delta\theta}{\overline{U}^2}, \tag{8}$$

where B is the Bulk Richardson Number and g is the acceleration of gravity. $\overline{T}$ is the ambient temperature at the geometric mean height of the Surface Boundary Layer, and $\overline{U}$ is the approximate wind speed at the same altitude. The potential temperature lapse in the Surface Boundary Layer is denoted by $\Delta\theta$, calculated from the surface potential temperature for the current grid and the potential temperature at the top of the mixing layer.

A neutral drag coefficient is determined from Barker and Baxter:[23]

$$C_N = \frac{1}{k} \ln\left(\frac{z_a}{z_o}\right), \tag{9}$$

where C_N is the drag coefficient, k is the Von Karman constant, z_a is the geometric mean height of the Surface Boundary Layer, and z_o is the surface roughness length.

The method of Barker and Baxter is then used to determine Monin-Obukhov length.[23] For stable, neutral, and slightly unstable conditions, the form,

$$L = \frac{z_a\ (1 - \beta B)}{k\ C_N \left[B - \left(\frac{R}{2\beta}\right) + \left(\frac{1-R}{\beta} B + \frac{R^2}{4\beta^2}\right)^{1/2}\right]}\ , \qquad (10)$$

is used where L is the Monin-Obukhov length and β and R are empirical constants.

Under more unstable conditions the approximation,

$$L = \frac{z_a}{B\ (0.471\ C_N - 1.045)}\ , \qquad (11)$$

is employed.

Surface Friction Velocity

The surface friction velocity characterizes frictional drag, wind shear, and vertical momentum transport in the Surface Boundary Layer. A logarithmic (neutral stability) wind profile is usually assumed in dispersion models so that surface friction velocity can be calculated from a simplified expression. The TRAC model employs the full analytical solution for friction velocity, which produces realistic, nonlogarithmic profile shapes during stable and unstable conditions.[24]

The exact expression reported by Schultz[25] is used for stable and neutral conditions:

$$u_* = \frac{k\ \overline{U}_z}{\ln\left(\frac{z}{z_o}\right) + 4.7\left(\frac{z}{L}\right)}\ , \qquad (12)$$

where $\overline{U}_z$ is the mean wind speed at a height z in the Surface Boundary Layer. The formula reduces to the traditional expression as $L \to \infty$ (stability approaches neutral).

The expression for unstable conditions is reported by Businger:[24]

$$u_* = \frac{k\ \overline{U}_z}{\ln\left(\frac{z}{z_o}\right) - \Psi_m}\ , \qquad (13)$$

where Ψ_m is a diabatic correction factor. Exact calculation of Ψ_m is computationally inefficient. A polynominal-fit approximation, developed by Schultz[25] is employed to overcome this problem:

$$\Psi_m = -0.312\left(\frac{z}{L}\right)^4 - 1.54\left(\frac{z}{L}\right)^3 - 2.81\left(\frac{z}{L}\right)^2 - 2.69\left(\frac{z}{L}\right) \qquad (14)$$

This approach requires only 25% of the computing time used by the full expression. It introduces an error of less than 3% in u_* over very rough surfaces (buildings and trees) and less than 1% over other surfaces.

Along-Flow Diffusion

Longitudinal turbulence in the mixing layer is parameterized using similarity formulas from Hanna et al.[10] During unstable conditions, turbulence is calculated from

$$\sigma_u = u_* \left(12 - 0.5\ \frac{z_i}{L}\right)^{1/3}\ , \qquad (15)$$

where σ_u is the along-wind turbulence parameter and z_i is the depth of the mixing layer above the grid surface. When the atmosphere is near-neutral, the formula,

$$\sigma_u = 2u_*\ \exp\left(\frac{-3fz_p}{u_*}\right)\ , \qquad (16)$$

is used, where z_p is the height of the puff centroid above the local grid surface and f is the Coriolis parameter. Under stable atmospheric conditions, turbulence intensity is calculated from

$$\sigma_u = 2u_*\ \left(1 - \frac{z_p}{z_i}\right). \qquad (17)$$

Along-wind diffusion is determined from longitudinal turbulence using universal conversion functions. Irwin's[14] best-fit approximations to Pasquill's[26] empirical results have been differentiated to provide a pseudo-Lagrangian formula for puff growth. For total puff travel distances less than 10^4 meters, the TRAC model determines rates of change of along-wind diffusion by

$$\frac{d\sigma_x}{dt} = \sigma_u \left(\frac{1 + 0.1674\, x_t^{.46}}{1 + 0.62\, x_t^{.46} + 0.0961\, x_t^{.92}} \right), \quad (18)$$

where σ_x is the along-wind diffusion parameter and x_t is the distance traveled by the puff along its non-linear trajectory since release. When total travel distance exceeds 10^4 meters, the diffusion parameter is more simply determined from

$$\frac{d\sigma_x}{dt} = 16.5\, \sigma_u\, x_t^{-1/2} \quad . \quad (19)$$

Across-Flow Diffusion

Across-flow diffusion is determined in a similar manner. The similarity formulas presented by Hanna et al. are used to parameterize cross-wind turbulence.[10] Latitudinal and longitudinal turbulence intensities are nearly equal during unstable conditions, so that Rocky Flats uses

$$\sigma_v = u_* \left(12 - 0.5\, \frac{z_i}{L} \right)^{1/3} \quad (20)$$

to estimate unstable cross-wind turbulence, where σ_v is the across-wind turbulence intensity. During near-neutral conditions, the cross-wind turbulence is calculated from

$$\sigma_v = 1.3\, u_* \exp\left(-2\, \frac{f z_p}{u_*} \right), \quad (21)$$

while the expression,

$$\sigma_v = 1.3\, u_* \left(1 - \frac{z_p}{z_i} \right), \quad (22)$$

is used during periods of stable atmospheric conditions.

Pseudo-Lagrangian diffusion rate formulas for across-wind diffusion were developed in the manner described in the preceding subsection, "Along-Flow Diffusion." For travel distances less than 10^4 meters, the rate of change of cross-wind diffusion is calculated from

$$\frac{d\sigma_y}{dt} = \sigma_v \left(\frac{1 + 0.1674\, x_t^{.46}}{1 + 0.62\, x_t^{.46} + 0.0961\, x_t^{.92}} \right), \quad (23)$$

where σ_y is the across-wind diffusion parameter. For travel distances greater than 10^4 meters, a simpler expression is used:

$$\frac{d\sigma_y}{dt} = 16.5\, \sigma_v\, x_t^{-1/2} \quad (24)$$

Vertical Diffusion

The TRAC model parameterizes vertical turbulence in the mixing layer with the method discussed in Hanna et al.[10] During unstable conditions, the convective scaling velocity (w_*) replaces friction velocity as the important vertical similarity parameter.[27]

The model uses the method of Panofsky et al. to calculate w_*:[9]

$$w_* = u_*\, k^{-1/3} \left(\frac{z_i}{-L} \right) \quad (25)$$

The mixing layer is divided into four sublayers for calculating vertical turbulence during unstable conditions. The Surface Boundary Layer is parameterized by

$$\sigma_w = 0.96\, w_* \left(\frac{3 z_p}{z_i} - \frac{L}{z_i} \right)^{1/3}, \quad (26)$$

where σ_w is the vertical component of turbulence. The mixing layer from the top of the Surface Boundary Layer to 40% of the mixing depth is characterized with

$$\sigma_w = 0.763 \left(\frac{z_p}{z_i}\right)^{0.175} , \quad (27)$$

while the layer to 96% of the mixing depth is characterized by

$$\sigma_w = 0.722 \left(1 - \frac{z_p}{z_i}\right)^{0.207} . \quad (28)$$

The top 4% of the mixing layer and all levels above the mixing depth are characterized by a constant turbulence intensity level during unstable conditions,

$$\sigma_w = 0.37\, w_* . \quad (29)$$

Surface friction velocity remains the important similarity parameter for vertical turbulence under non-convective conditions. Near-neutral turbulence is characterized by

$$\sigma_w = 1.3\, u_* \exp\left(-2 \frac{fz_p}{u_*}\right) . \quad (30)$$

During stable conditions, the expression,

$$\sigma_w = 1.3\, u_* \left(1 - \frac{z_p}{z_i}\right) , \quad (31)$$

is used.

Next, the vertical component of turbulence is converted to vertical fluctuation angle,[22]

$$\sigma_\phi = \frac{\sigma_w}{\overline{U}_p} , \quad (32)$$

where σ_ϕ is the standard deviation of vertical wind direction and $\overline{U}_p$ is the mean horizontal wind speed at the puff centroid height.

Vertical direction fluctuations are converted to the rate of change of vertical diffusion using differentiated forms of Draxler's equations.[28] During unstable conditions, the model uses

$$\frac{d\sigma_z}{dt} = \frac{\frac{x_t}{t}\, \sigma_\phi\, (1 + 0.02t^{1/2})}{(1 + 0.0016t + 0.08t^{1/2})} , \quad (33)$$

where σ_z is the vertical diffusion coefficient and t is the total puff travel time since release.

Under neutral and stable conditions, the model uses

$$\frac{d\sigma_z}{dt} = \frac{\frac{x_t}{t}\, \sigma_\phi\, (1 + 0.0043t^{-.81})}{(1 + 0.0005t^{1.62} + 0.456t^{-.81})} . \quad (34)$$

Coordinate Transform

The total diffusion growth during a time step is calculated from

$$\Delta\sigma_x = \Delta t \cdot \frac{d\sigma_x}{dt} , \quad (35)$$

$$\Delta\sigma_y = \Delta t \cdot \frac{d\sigma_y}{dt} , \quad (36)$$

and

$$\Delta\sigma_z = \Delta t \cdot \frac{d\sigma_z}{dt} , \quad (37)$$

where $\Delta\sigma_x$, $\Delta\sigma_y$, and $\Delta\sigma_z$ are incremental plume growths during the time step and Δt is the time step period.

Vector analysis is used to convert the sigmas to the local puff coordinate system. First, a vector is created with direction coordinates ($\Delta\sigma_x$, $\Delta\sigma_y$, $\Delta\sigma_z$). These coordinates are rotated horizontally in a transform to the standard (x, y, z) system. Then the vector is projected onto the local puff axes, resulting in sigmas for the x′, y′, z′ reference frame.

NET PUFF GROWTH AND SHAPE

Final puff growth during a time step is determined independently for each puff axis. Either divergence/shear or diffusion is selected to dominate growth

along an axis, depending on which mechanism results in the greatest spread. Thus, divergence/shear can dominate some parts of a puff, while diffusion controls the growth of other portions.

The model guarantees a positive diffusion rate, even under calm conditions. Therefore, the puff will grow in all three dimensions during each time step (even in a convergent wind field) and entropy will be maintained.

The width of a puff during a time step is described by

$$\sigma_{xo} = \sigma_{xo}' + \Delta\sigma_x \quad , \qquad (38)$$

$$\sigma_{yo} = \sigma_{yo}' + \Delta\sigma_y \quad , \qquad (39)$$

and

$$\sigma_{zo} = \sigma_{zo}' + \Delta\sigma_z \quad , \qquad (40)$$

where σ_{xo}, σ_{yo}, and σ_{zo} are the puff standard deviations along the local axes measured at the puff centroid and σ_{xo}', σ_{yo}', and σ_{zo}' are the puff standard deviations at the beginning of the time step.

Because the puffs are ellipsoidal, sigmas vary continuously across the puff surface. As shown in Figure 7, sigmas are maximized along their related axes (e.g., σ_y has a maximum value of σ_{yo} at the y' axis). Sigmas decrease with distance from their related axes, reaching a minimum of 0 at adjacent puff axes. Thus, the sigma values used to calculate concentration will depend both on the width of

FIGURE 7. Cross Section of an Ellipsoidal Puff. The variation of puff width (standard deviation) as a function of distance from the centroid is illustrated.

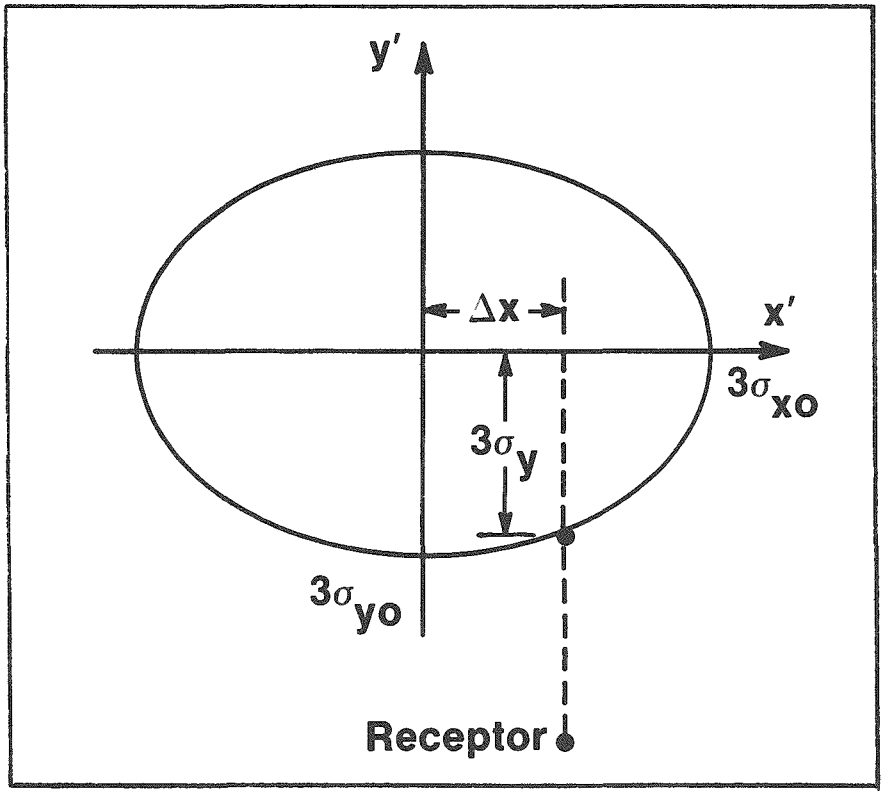

the puff at the axes (the maximum sigma values) and the relative position between a receptor and the puff.

The $\pm 3\sigma$ envelope of the puff is defined by

$$\frac{x^2}{\sigma_{xo}^2} + \frac{y^2}{\sigma_{yo}^2} + \frac{z^2}{\sigma_{zo}^2} = 9 \quad , \quad (41)$$

where x, y, and z are the coordinates of points that lie on the outer puff surface. Using this relationship, sigmas for specific receptor-puff relationships are calculated as

$$\sigma_x = \frac{\sigma_{xo}}{3} \left(9 - \frac{\Delta y^2}{\sigma_{yo}^2} - \frac{\Delta z^2}{\sigma_{zo}^2}\right)^{1/2} \quad , \quad (42)$$

$$\sigma_y = \frac{\sigma_{yo}}{3} \left(9 - \frac{\Delta x^2}{\sigma_{xo}^2} - \frac{\Delta z^2}{\sigma_{zo}^2}\right)^{1/2} \quad , \quad (43)$$

and

$$\sigma_z = \frac{\sigma_{zo}}{3} \left(9 - \frac{\Delta x^2}{\sigma_{xo}^2} - \frac{\Delta y^2}{\sigma_{yo}^2}\right)^{1/2} \quad , \quad (44)$$

where σ_x, σ_y, and σ_z are the puff-receptor-specific sigmas and Δx, Δy, and Δz are the distances from the puff centroid to the projections of the receptor location on the puff axes.

BOUNDARY EFFECTS

Surface Boundary

Puffs in the TRAC model interact with grid surfaces through wet deposition, gravitational settling, dry deposition, and reflection. Wet deposition processes are assumed to affect the entire puff (wash-out is assumed) and act to deplete the puff mass without changing its shape or position. Puff tilt, through gravitational settling of particulates, is incorporated directly into the trajectories of the tracer particles.

Dry deposition and reflection act near the puff-surface interface. Dry deposition removes material only from the lowest layers of the puff; mass distribution in the upper portions remains unaffected. Low-level turbulence results in the immediate resuspension of materials not captured by the surface. This process also affects only the lowest layers of the puff. The result is an increasingly non-Gaussian distribution in the lowest portion of the puff during periods of surface impaction.

The TRAC model evaluates the effects of dry deposition and surface impaction on puff shape and mass distribution using Overcamp's partial reflection approach.[29] The method is similar to the standard reflection formula,[21] except that a surface reflection coefficient is incorporated. Using this term, the model reflects from the surface only that material not lost through dry deposition.

Overcamp's formulas assume steady-state conditions and thus cannot be used in the TRAC model. A Lagrangian approach to surface reflection has been developed, which accepts variable surface and puff conditions. The method assumes that deposition and reflection affect only the portion of a puff below the centroid.

Because the puff coordinate system is not orthogonal and not, in general, aligned with the grid surface, a reflection term must be evaluated along each puff axis. The results are

$$\alpha_x = \frac{Q}{Q_o} \frac{\left\{1 + \exp\left[-2\left(\frac{h_x}{\sigma_{xo}}\right)^2\right]\right\} - 1}{\exp\left[-2\left(\frac{h_x}{\sigma_{xo}}\right)^2\right]}, \quad (45)$$

$$\alpha_y = \frac{Q}{Q_o} \frac{\left\{1 + \exp\left[-2\left(\frac{h_y}{\sigma_{yo}}\right)^2\right]\right\} - 1}{\exp\left[-2\left(\frac{h_y}{\sigma_{yo}}\right)^2\right]}, \quad (46)$$

and

$$\alpha_z = \frac{Q}{Q_o} \frac{\left\{1 + \exp\left[-2\left(\frac{h_z}{\sigma_{zo}}\right)^2\right]\right\} - 1}{\exp\left[-2\left(\frac{h_z}{\sigma_{zo}}\right)^2\right]}, \quad (47)$$

where α_x, α_y, and α_z are the surface reflection coefficients along the x′, y′, and z′ axes, Q is the mass of the puff including losses caused by dry deposition, Q_o is the mass of the puff excluding dry deposition losses. Distances h_x, h_y, and h_z are measured from the grid surface to the puff centroid along the respective puff axes. Because the reflection coefficients are recalculated for each puff and each receptor at every time step, the Lagrangian effects of varying deposition rate, surface characteristics, puff shape, and puff-surface distance are realistically addressed.

Upper and Horizontal Boundaries

The TRAC model does not consider reflection effects at the side and upper boundaries of the study area. Horizontal motion and dispersion of a puff between valley walls is restricted by the mass conservation requirements of the windfield module. Puff material cannot transport fictitiously through an obstacle, but can surround a terrain feature if a path is available.

The only restriction to vertical motion above the surface occurs at the top of the mixing layer. Puff tracer particles are not allowed to move up or down through the inversion marking the mixing depth. However, puffs are allowed to react to changes in the inversion lid (such as fumigation).

RECEPTOR CONCENTRATIONS

Pollutant concentrations at receptor grids are calculated from a form of the Gaussian puff equation, modified to treat partial reflection along each of the puff axes:

$$\chi = \frac{Q_o}{(2\pi)^{1/2}\,\sigma_x\sigma_y\sigma_z} \tag{48}$$

$$\left\{\exp\left[-\frac{1}{2}\left(\frac{x-h_x}{\sigma_x}\right)^2\right] + \alpha_x \exp\left[-\frac{1}{2}\left(\frac{x+h_x}{\sigma_x}\right)^2\right]\right\}$$

$$\left\{\exp\left[-\frac{1}{2}\left(\frac{y-h_y}{\sigma_y}\right)^2\right] + \alpha_y \exp\left[-\frac{1}{2}\left(\frac{y+h_y}{\sigma_y}\right)^2\right]\right\}$$

$$\left\{\exp\left[-\frac{1}{2}\left(\frac{z-h_z}{\sigma_z}\right)^2\right] + \alpha_z \exp\left[-\frac{1}{2}\left(\frac{z+h_z}{\sigma_z}\right)^2\right]\right\}$$

where χ is the pollutant concentration at the receptor.

OTHER MODEL COMPONENTS AND FUTURE EFFORTS

The TRAC dispersion model includes modules to treat other atmospheric effects. Surface roughness lengths are calculated dynamically for each grid. Microscale terrain complexity, snow cover, seasonal growth, and 25 categories of surface cover are combined to provide a realistic surface roughness field.

Wash-out algorithms are included for several classes of particulates and gases. Real-time, grid-by-grid precipitation rates are generated as part of the windfield code, allowing a realistic treatment of wet removal processes. The model's dry deposition algorithm develops deposition velocities based on near-surface concentration gradients, surface characteristics, low-level turbulence intensities, and pollutant type. Gravitational settling of small- to moderate-sized particles is treated with Stoke's formulas; large particles are settled ballistically.

Resuspension is treated by tracking grid-by-grid integrated deposition. When the mass deposited in a grid reaches a threshold level, the grid is added to a list of area sources. Wind erosion emission rates are calculated for the grid during all following timesteps until the deposition mass again falls below the threshold.

Algorithms for assessment of radionuclide releases include ingrowth and decay of fission products, external dosimetry, and inhalation dosimetry.

Input routines are interactive and include extensive on-screen help text. A catalog of default characteristics for potential release situations is maintained—the user is queried for necessary changes.

Output includes trajectory maps, regional isopleth maps for concentration, dose, deposition, and tabular output for selected receptors.

These model modules will be discussed in detail in subsequent publications.

Future upgrades will incorporate modules for evaluation of building effects on transport and diffusion, ground plane irradiation, food-chain pathway analysis, and statistical analysis of model outputs.

SUMMARY

The TRAC dispersion model has been developed to treat mesoscale transport and dispersion over complex terrain. Utilizing topographic, surface cover, and available meteorological information, the code produces three-dimensional, time- and space-varying windfields. Puffs are transported along nonlinear trajectories through these flow fields. Tracer "particles" are used to identify the envelopes of puffs. Although computationally ellipsoidal and Gaussian, puffs can develop arbitrary shapes and pollutant distributions in response to transport, divergence/shear, diffusion and removal mechanisms.

REFERENCES

1. J. R. Bowers, J. R. Bjorklund, and C. S. Cheney, *Industrial Source Complex (ISC) Dispersion Model User's Guide* (Volume 1), U.S. Environmental Protection Agency Report EPA-450/4-79-030, U.S. EPA, Research Triangle Park, NC (1979)

2. E. W. Burt, *Valley Model User's Guide*, U.S. Environmental Protection Agency Report EPA-450/2-77-018, U.S. EPA, Research Triangle Park, NC (1977)

3. R. W. Moore, C. F. Baes III, L. M. McDowell-Boyer, A. P. Watson, F. O. Hoffman, J. C. Pleasant, and C. W. Miller, *AIRDOS-EPA: A Computerized Methodology for Estimating Environmental Concentrations and Dose to Man From Airborne Releases of Radionuclides,* Oak Ridge National Laboratory Report ORNL-5532, ORNL, Oak Ridge, TN (1979)

4. K. S. Rao and L. Satterfield, *MPTER-DS: The MPTER Model Including Deposition and Sedimentation - User's Guide,* U.S. Environmental Protection Agency Report EPA-600/8-82-024, U.S. EPA, Research Triangle Park, NC (1982)

5. P. H. Gudiksen, *ASCOT Data From the 1979 Field-Measurement Program in Anderson Creek Valley, California,* Lawrence Livermore National Laboratory Report UCID-18874 ASCOT-80-9, LLNL, Livermore, CA (1980)

6. E. E. Uthe, "Application of Surface Based and Airborne Lidar Systems for Environmental Monitoring," *J. Air Pollution Control Association, 33:12,* pp 1149-1155, (1983)

7. C. M. Sheih, "A Puff Pollutant Dispersion Model With Wind Shear and Dynamic Plume Rise," *Atmospheric Environment, 12,* pp 1933-1938, (1978)

8. T. Yamada, "Prediction of the Nocturnal Surface Inversion Height," *Journal of Applied Meteorology, 18,* pp 526-531, (1979)

9. H. A. Panofsky, H. Tennekes, D. H. Lenschow, and J. C. Wyngaard, "The Characteristics of Turbulent Velocity Components in the Surface Layer Under Convective Conditions," *Boundary-Layer Meteorology, 11,* pp 355-361, (1977)

10. S. R. Hanna, G. A. Briggs, and R. P. Hosker, Jr., *Handbook on Atmospheric Diffusion,* U.S. Department of Energy Document DOE/TIC-11223, Technical Information Center, Oak Ridge, TN (1982)

11. M. A. Fosberg, W. E. Marlatt, and L. Krupnak, *Estimating Flow Patterns Over Complex Terrain,* U.S.D.A. Forest Service Research Paper RM-162, U.S. Department of Agriculture, Fort Collins, CO (1976)

12. G. E. Anderson, " Mesoscale Influences on Wind Fields," *J. Applied Meteorology, 10,* pp 377-386 (1971)

13. M. A. Fosberg, A. Rango, and W. E. Marlatt, "Wind Computations From the Temperature Field in an Urban Environment," *Proc. of the Conference on Urban Environments and Second Conference on Biometeorology*, Oct. 31–Nov. 2, 1972, Philadelphia, PA, pp 5-7.

14. J. S. Irwin, "Estimating Plume Dispersion–A Recommended Generalized Scheme," *Preprints of Fourth Symposium on Turbulence, Diffusion, and Air Pollution*, Reno, NV, Jan. 15-18, 1979, American Meteorological Society, pp 62-69.

15. R. Lange, "Modeling a Multiple Tracer Release Experiment During Nocturnal Drainage Flow in Complex Terrain," *Preprints of the Second Conference on Mountain Meteorology*, Steamboat Springs, CO, Nov. 9-12, 1981, American Meteorology Society, pp 245-252.

16. B. W. Atkinson, *Meso-scale Atmospheric Circulations*, Academic Press, New York (1981)

17. G. J. Haltiner and F. L. Martin, *Dynamical and Physical Meteorology*, McGraw-Hill Book Company, New York (1957)

18. A. S. Monin and A. M. Obukhov, "Basic Laws of Turbulent Mixing in the Atmosphere Near the Ground," *Tr. Akad. Nauk. SSSR Geofiz. Inst., 24*, pp 163-187 (1954)

19. A. S. Monin and S. S. Zilitinkevich, "Similarity Theory and Resistance Laws for the Planetary Boundary Layer," *Boundary-Layer Meteorology, 7*, pp 391-397 (1974)

20. S. R. Hanna, "Applications in Air Pollution Modeling," *Atmospheric Turbulence and Air Pollution Modeling*, F. T. M. Nieuwstadt and H. van Dop, eds., D. Reidel Publishing Company, Boston, MA, pp 275-310 (1982)

21. D. B. Turner, *Workbook of Atmospheric Dispersion Estimates*, U.S. Environmental Protection Agency Report AP-26, U.S. EPA, Research Triangle Park, NC (1970)

22. R. R. Draxler, "Estimating Vertical Diffusion From Routine Meteorological Tower Measurements," *Atmospheric Environment, 13*, pp 1559-1564 (1979)

23. E. H. Barker and T. L. Baxter, "A Note on the Computation of Atmospheric Surface Layer Fluxes for Use in Numerical Modeling," *J. of Applied Meteorology, 14*, pp 620-622 (1975)

24. J. A. Businger, *Workshop on Micrometeorology*, American Meteorological Society, Boston, MA (1973)

25. P. Schultz, "Estimation of Surface Stress From Wind," *Boundary-Layer Meteorology, 17*, pp 265-267 (1979)

26. F. Pasquill, *Atmospheric Dispersion Parameters in Gaussian Plume Modeling: Part II. Possible Requirements for Change in the Turner Workbook Values*, U.S. Environmental Protection Agency Report EPA-600/4-76-0306, U.S. EPA, Research Triangle Park, NC (1976)

27. J. W. Deardorff, "A Three Dimensional Numerical Investigation of the Idealized Planetary Boundary Layer," *J. Geophys. Fluid Dyn., 1*, pp 377-410 (1970)

28. R. R. Draxler, "Determination of Atmospheric Diffusion Parameters," *Atmospheric Environment, 10*, pp 99-105 (1976)

29. T. J. Overcamp, "A General Gaussian Diffusion-Deposition Model for Elevated Point Sources," *Journal of Applied Meteorology, 15*, pp 1167-1171 (1976)